2.5 THE RELATION BETWEEN SLOPE FLOW SYSTEMS AND CONVECTIVE BOUNDARY LAYERS IN STEEP TERRAIN

C. Reuten[1] *, D.G. Steyn[1], K.B. Strawbridge[2], and P. Bovis[1]
[1]Atmospheric Science Program, The University of British Columbia, Vancouver, BC, Canada
[2]Air Quality Process Research Division, Meteorological Service of Canada, Egbert, ON, Canada

1. INTRODUCTION

Slope flows are crucial for the transport of air pollutants in regions of complex terrain. Daytime slope flow systems often exhibit a two-layer structure of upslope flow in the bottom layer and return flow in the upper layer. The relationship of this two-layer structure with the convective boundary layer (CBL) appears to have been of little interest in the past. Based on few observations and modelling results the common understanding is that daytime upslope flows vent air pollutants out of the CBL into the free atmosphere. Return flows are understood to be either very small or occur above the top of the boundary layer. Investigations primarily concentrate on the fate of the pollutants after having been vented into the free atmosphere, like re-entrainment into the boundary layer after having been advected to a different region.

During the air pollution field study Pacific 2001 in the Lower Fraser Valley, British Columbia, Canada, we studied slope flow mechanisms by taking measurements of wind speed, lidar backscatter of particulate matter, temperature, and specific humidity. The results presented here are based on measurements taken on July 25-26, 2001 during weak synoptic winds, clear skies, and strong daytime solar heating.

Measurements of the three air flow components were performed with a Doppler sodar at the foot of a SSE-facing slope with an average angle of 19° and a ridge height of approximately 1000m. Flows were imbedded in a shallow CBL with a maximum mean height of approximately 900m. The maximum scanning height of the sodar was 1000m which allowed us to investigate the flow structure in the entire CBL. The vertical resolution was 20 - 50m. At a nearby site in the adjacent plain, a RASCAL (Rapid Acquisition Scanning Aerosol Lidar) and a tethersonde were used to measure the backscatter of particulate matter and the temperature, wind speed and direction, and specific humidity, respectively. RASCAL data was obtained over a 12km range at a resolution of 3m along the beam axis and a scan speed of 0.1 degrees per second resulting in each elevation scan taking approximately 5 minutes to acquire.

* *Corresponding author address:* Christian Reuten, The University of British Columbia, Dept. of Earth and Ocean Sciences, 6270 University Blvd., Vancouver, BC V6T1Z4, Canada; e-mail:creuten@eos.ubc.ca

2. OBSERVATIONS

2.1 *Approach*

Lidar scans were performed above the entire beam range of the sodar with very high frequency. An algorithm was used similar to Strawbridge et al. (2001) to determine the top of the backscatter boundary layer. On the other hand, the tethersonde provided only point measurements almost 3000m distant from the sodar and the slope, the time of measurements at various heights was more uncertain, and the interpretation of the potential temperature and specific humidity profiles is difficult.

Figure 1 shows a lidar scan with the top of the backscatter boundary layer and the tethersonde profiles of potential temperature and specific humidity, which indicate the top of the thermal (convective) boundary layer, in one graph. The discrepancy between the two can be explained by noting that the lidar scan is basically a measurement in an instant of time towards the end of the 40-minutes tethersonde flight. Furthermore, the position of the tethersonde was 500m left of the origin of Figure 1. Therefore, measurements made by the lidar over the plane adjacent to the slope must be extrapolated to the position of the tethersonde. Finally, a modification of the top of the backscatter boundary layer due to a correction of the vertical angle is not shown in the scan.

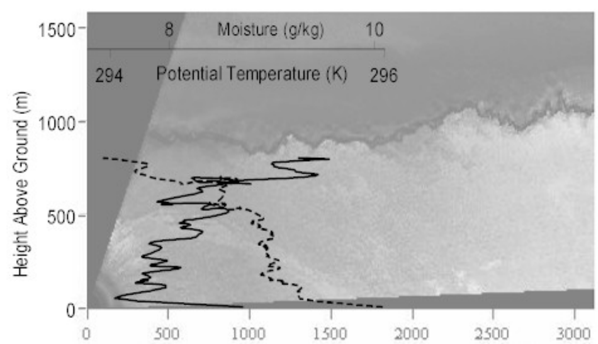

Figure 1: Tethersonde profiles of potential temperature (solid line) and specific humidity (dashed line) measured on July 26, 2001 from 1448-1528 (PDT) superimposed on a section of a lidar scan taken on July 26, 2001 at 1517 (PDT). The bold line on top of the light-shaded aerosol layer indicates the top of the backscatter boundary layer.

Figure 2 shows the relationship between the top of the backscatter boundary layer extrapolated from the scanning lidar system data and the thermal (convective) boundary layer determined from tethersonde measurements of potential temperature and specific humidity over a 75-minute morning period. The range above and below the data points indicates the maximum range due to overshooting thermals and entrainment.

Figure 2 demonstrates that thermal boundary layer (as indicated by the grey areas) and backscatter boundary layer (as indicated by the data points with maximum range) are in good agreement. We can therefore use the more abundant lidar data to establish the relationship between the slope flow system and the CBL.

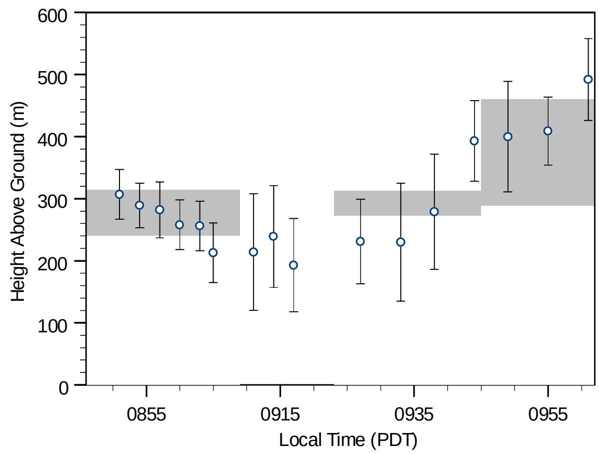

Figure 2: Time development of entrainment zone of thermal boundary layer (grey area) and backscatter boundary layer (data points with maximum range due to overshooting thermals and entrainment) on July 25, 2001.

2.2 *Slope Flow System Versus Boundary Layer*

The U- and V-component of the wind measurements with the Doppler sodar were rotated to be perpendicular and parallel to the direction of the steepest slope, respectively. The W-component remained vertical.

Figure 3 shows a time-height section of the upslope wind component over a 4-hour morning period. Vectors are composed of a vertical and a slope-parallel component. Vectors pointing to the right correspond to upslope flows, vectors pointing to the left are associated with return flows in the down-slope direction. Lidar measurements of the top of the CBL were averaged over the entire horizontal spread of the sodar beam (29° from the vertical). The results are superimposed on the vector plot in Figure 3. Similarly to Figure 2, the range for each data point indicates minimum and maximum values of the CBL height within the averaging area.

As early as 0900 local daylight saving time, an upslope wind starts to build up, which grows to a strength of about 3-5 m/s and a depth of approximately 400 m in the later morning. At the same time, a return flow of equal strength and depth starts to build up. Upslope flow and return flow both lie within the CBL. The depth of upslope flow layer and the return flow layer aloft are each approximately half the depth of the CBL.

Figure 4 shows a 2-hour afternoon period on the following day in the same format as Figure 3. The same tendency can be seen here although the quality of data is not as good as in Figure 3. This is due to difficulty of the sodar to resolve data near its maximum reach of 1000m and a smaller data set.

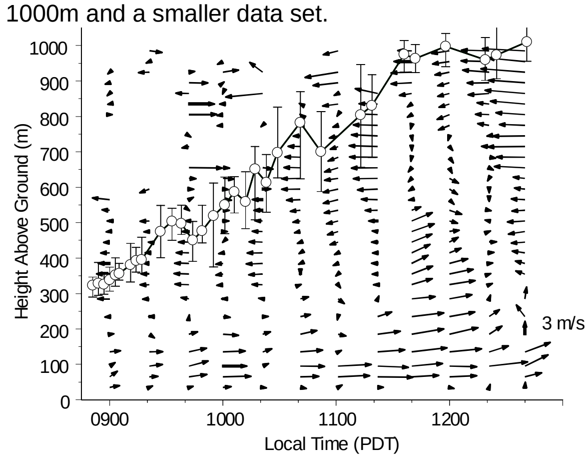

Figure 3: Slope component of wind speed measured with Doppler sodar (right = upslope) at different heights over a 4-hour morning period on July 25, 2001. The data for the top of the convective layer based on the lidar measurements are superimposed. The range for each data point indicates maximum rise of thermals and minimum height of entrainment within the horizontal spacing due to beam spreading of the Doppler sodar.

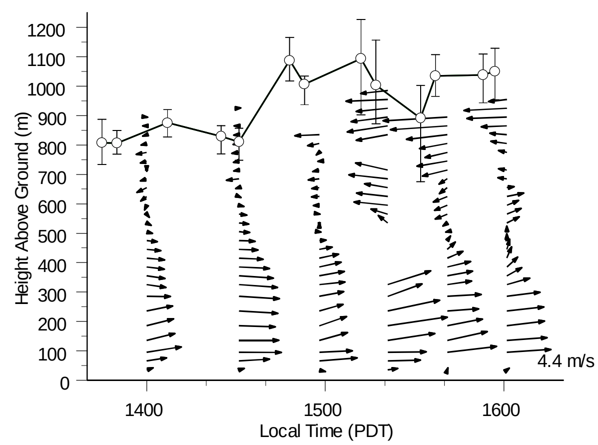

Figure 4: Same as Figure 3 but for afternoon of July 26, 2001.

Figure 5 displays the mean of all measurements in the time period of Figure 3 for a given height (solid curve). The dashed curves show the standard deviation of the measurements. For each sodar scan, the slope flow components were normalized by the maximum upslope speed. The height was normalized by the average height of the CBL determined from the lidar scans. The horizontal dashed line indicates the top of the CBL.

Despite the large scatter of data it can be clearly seen that the upslope flow occurs in the bottom half of the CBL and the return flow occurs in the upper half below the average top of the boundary layer. A direct comparison of the top of the upslope flow and top of the return flow with the top of the CBL is shown in Figure 6.

The top of the upslope flow scatters around the dashed line indicating half the height of the CBL. The top of the return flow scatters along the solid line indicating the height of the top of the CBL.

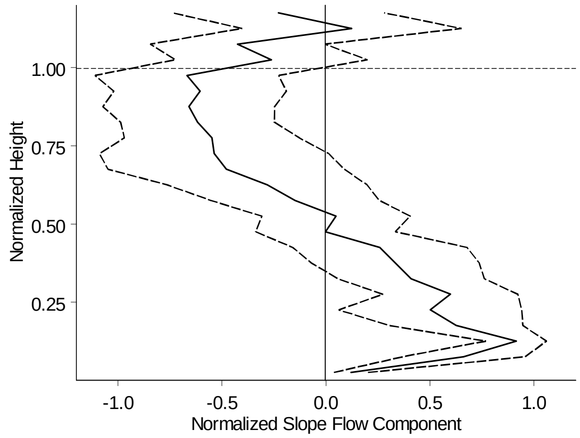

Figure 5: Normalized slope flow component versus normalized height for same 4-hour period as in Figure 3. The solid curve shows the time average for each height, dashed curves indicate standard deviation, the dashed horizontal line is the top of CBL.

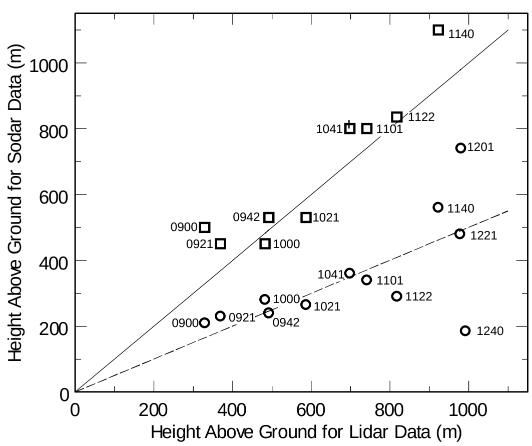

Figure 6: Comparison of top of upslope flow (circles) and top of return flow (squares) with the top of the CBL.

From Figure 5 and Figure 6 it can be seen that the top of the return flow appears to lie slightly above the top of the CBL. The two heights match more closely if height is normalized by maximum rather than average values of the CBL height within the sodar's beam spread, averaged over the sodar's integration time. In the latter case, the top of the CBL would be defined as the maximum height of overshooting thermals.

2.3 *Shape of Slope Flow System*

The solid curve of Figure 5 is reproduced in Figure 7, re-normalized to the maximum upslope speed. Figure 7 illustrates the velocity profile and compares it with analytical profiles. The thin solid line is composed of two parabolas. Parabolic best fits have previously been applied to valley flows, Atkinson (1981). The dashed line shows a Prandtl profile assuming that the weak return flow of the Prandtl profile occurs within the CBL, the dash-dotted line shows a Prandtl profile for the upslope flow filling the entire CBL. While the first Prandtl profile closely matches the data in the bottom half of the CBL it fails in the upper half. The other two profiles generally do not provide good approximations to the data.

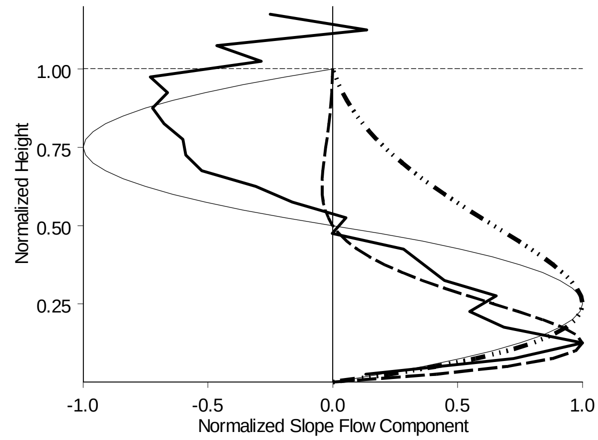

Figure 7: Normalized time average of slope flow for each height (bold solid), parabolic profile (thin solid line), Prandtl profile with return flow within CBL (dashed line) and with upslope flow filling entire CBL (dotted line).

2.4 *Mass Flux*

The dynamic mass flux can be approximated by

$$M = \int_0^h \rho(z) b \frac{ds}{dt} dz \cong \rho b \int_0^h V(z) dz \cong \rho b \sum_j V(z_j) \cdot \Delta z_j$$

where b is the width of flow, s the length in slope flow direction, $V(z) = ds/dt$ the upslope velocity at height z, h the height of the CBL; the density $\rho(z) \cong \rho$ is assumed to be approximately constant within the CBL. $V(z_j)$ denotes the slope wind component at height z_j of the j-th layer, and Δz_j is the depth of that layer.

Figure 8 shows upslope, downslope, and residual dynamic mass fluxes for a flow width of $b = 1000m$ and density $\rho = 1.2\,kg/m^3$. The mass fluxes appear unbalanced and unsteady over short periods of time. However, over the entire morning period the mass fluxes balance rather well. The average values are:

Upslope flux: + 603 x 10^3 kg/s
Downslope flux: - 535 x 10^3 kg/s
Sum: + 67 x 10^3 kg/s (11% of upslope flux)

Dynamic mass flux of the downslope flow balances approximately 90% of the mass flux of the upslope flow. The discrepancy of 67x10^3kg/s could be due to uncertainties in the data. This rough mass balance between upslope flow and return flow indicates that the slope flow system we observed could be a closed circulation.

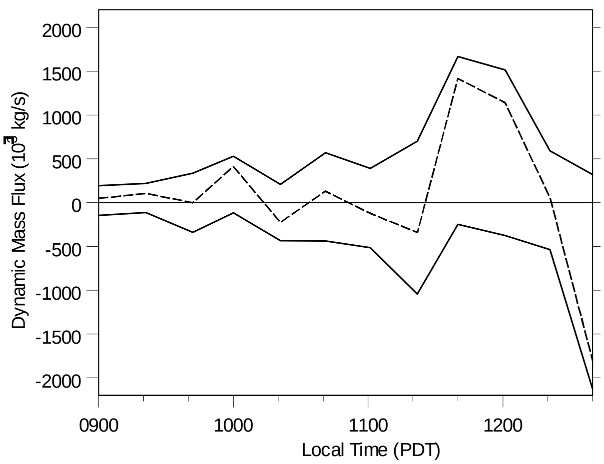

Figure 8: Dynamic mass fluxes for a flow width of 1 km for the same time period as in Figure 3. The upper solid curve shows upslope mass fluxes (positive), the lower solid curve downslope mass fluxes (negative). The sum of both (residual) is represented by the dashed line.

3. COMPARISON WITH OTHER INVESTIGATIONS

Observations of slope flow systems generally show upslope flows within the CBL, with return flows aloft (Wenger (1923), Davidson (1961) as cited in Atkinson (1981), Mendonca (1969), Kuwagata and Kondo (1989), Koßmann (1998)), though some of the earlier studies do not identify the CBL top. Figure 7 shows how the profile predicted by Prandtl's (1942) theoretical model compares with our observations. The large-eddy simulation performed by Schumann (1990) reveals slope flow circulations similar to Prandtl's predictions with generally weak return flows. The temperature structure indicates that the depth of the upslope flow agrees well with the depth of the CBL and that the return flow occurs above the top of the CBL. Scale model (tank) studies of slope flow systems show varied behaviour. Deardorff and Willis (1987), Mitsumoto (1989), and Chen et al. (1996) show slope upslope flow layers filling the entire CBL with return flows aloft, while Deardorff and Willis (1987) find a return flow layer below the top of the CBL under conditions of homogeneous heating.

4. SUMMARY AND CONCLUSIONS

Our observations show strong daytime upslope flows paired with often equally strong and deep return flows. Most remarkably, we observed that the return flows occurred below the mean top of the boundary layer. Depths of up to 500 m each for the upslope and the return flow and maximum values of the wind component parallel to the slope of up to 5m/s were observed. The normalized slope flow velocity profile remained fairly constant over a period of four hours. The Prandtl profile of slope flows closely matches our measured velocity profiles in the bottom half for the upslope flows. However, in the upper half the weak return flow of the Prandtl model fails to match our observations. Over a 4-hour morning period the dynamic mass flux of the return flow was shown to approximately balance the mass flux of the upslope flow.

These observations show that air pollutants can remain trapped under the top of the boundary layer rather than being vented into the free atmosphere, resulting in higher concentrations of air pollutants than previously expected.

5. ACKNOWLEDGEMENTS

Partial funding support was provided by NSERC and CFCAS and also by Environment Canada under the Pacific 2001 project.

6. REFERENCES

Atkinson, B. W., 1981: “Meso-scale atmospheric circulations”, Academic Press, London.

Chen, R.-R., N. S. Berman, D. L. Boyer, and H. J. S. Fernando, 1996: “Physical model of diurnal heating in the vicinity of a two-dimensional ridge”, J. Atmos. Sci., 53(1), 62-85.

Davidson, B., 1961: “Local wind circulations: final report”, Vol. II, Studies of the field of turbulence in the lee of mountain ridges and tree lines. Contract no. DA-36-039-sc-84939, College of Engineering, Research Division, New York University.

Deardorff, J. W., and G. E. Willis, 1987, “Turbulence within a baroclinic laboratory mixed layer above a sloping surface”, J. Atmos. Sci., 44(4), 772-778.

Koßmann, M., 1998: “Einfluß orographisch induzierter Transportprozesse auf die Struktur der atmosphärischen Grenzschicht und die Verteilung von Spurengasen”, Dissertation, Fakultät für Physik der Universität Karlsruhe (TH), Karlsruhe, Germany.

Kuwagata, T., and J. Kondo, 1989: “Observations and modeling of thermally induced upslope flow”, Bound.-Lay. Meteorol., 49, 265-293.

Mendonca, B., 1969: “Local wind circulation on the slopes of Mauna Loa”, J. Appl. Meteor., 8, 533-541.

Mitsumoto, S., 1989: “A laboratory experiment on the slope wind”, J. Met. Soc. Japan, 67 (4), 565-574.

Prandtl, L., 1942: “Führer durch die Strömungslehre”, Vieweg und Sohn, Braunschweig.

Schumann, U., 1990: “Large-eddy simulation of the upslope boundary layer”, Q. J. R. Met. Soc., 116, 637-670.

Strawbridge, K.B., M. Travis, and M. Harwood, 2001: “Preliminary results from scanning lidar measurements of stack plumes during winter/summer”, Proceedings of Laser Radar: Ranging and Atmospheric Lidar Techniques III. Editor: Manfred Ehlers. SPIE Vol. 4546. Toulouse, France.

Wenger, R., 1923: “Zur Theorie des Berg- und Talwindes”, Met. Zeitschr., 40, 193-204.